Role of a Dynamic Loop in Cation Activation and Allosteric Regulation of Recombinant Porcine Fructose-1,6-bisphosphatase[†,‡]

Jun-Yong Choe, Bradley W. Poland,[§] Herbert J. Fromm, and Richard B. Honzatko*

Department of Biochemistry and Biophysics, Iowa State University, Ames, Iowa 50011

Received May 13, 1998; Revised Manuscript Received June 24, 1998

ABSTRACT: A disordered loop (loop 52−72, residues 52−72) in crystal structures of fructose-1,6-bisphosphatase (FBPase) has been implicated in regulatory and catalytic phenomena by studies in directed mutation. A crystal structure of FBPase in a complex with three zinc cations and the products fructose 6-phosphate (F6P) and phosphate (P_i) reveals loop 52−72 for the first time in a well-defined conformation with strong electron density. Loop 52−57 interacts primarily with the active site of its own subunit. Asp68 of the loop hydrogen bonds with Arg276 and a zinc cation located at the putative potassium activation site. Leu56 and Tyr57 of the loop pack against hydrophobic residues from two separate subunits of FBPase. A mechanism of allosteric regulation of catalysis is presented, in which AMP, by binding to its allosteric pocket, displaces loop 52−72 from the active site. Furthermore, the current structure suggests that both the α- and β-anomers of F6P can be substrates in the reverse reaction catalyzed by FBPase. Mechanisms of catalysis are proposed for the reverse reaction in which Asp121 serves as a catalytic base for the α-anomer and Glu280 serves as a catalytic base for the β-anomer.

Fructose-1,6-bisphosphatase (FBPase,[1] EC 3.1.3.11) plays a central role in gluconeogenesis, hydrolyzing fructose 1,6-bisphosphate ($F16P_2$) to fructose 6-phosphate (F6P) and phosphate (P_i) (*1*−*6*). The enzyme is inhibited allosterically by AMP, the binding of which is cooperative with a Hill coefficient of approximately 2 (*7*−*9*). The regulator fructose 2,6-bisphosphate ($F26P_2$) is a potent inhibitor, which binds to the active site competitively with respect to the substrate $F16P_2$ (*10*−*12*). FBPase requires divalent cations (Mg^{2+}, Mn^{2+}, and/or Zn^{2+}) for activity, and certain monovalent cations (K^+, NH_4^+, and Tl^+) further enhance catalysis (*3*, *5*, *13*). Plots of enzyme activity as a function of divalent cation concentration are sigmoidal at pH 7.5 (Hill coefficient of approximately 2) and hyperbolic at pH 9.6 (*8*, *14*). The mammalian enzyme is a homotetramer and exists in distinct conformational states (T and R), depending on the relative concentrations of active site and allosteric site ligands (*15*). AMP and $F26P_2$ synergistically stabilize the T state conformation, which is an inactive form of the enzyme. $F16P_2$ stabilizes the R state (kinetically active conformer).

Even though the enzyme from mammalian sources has been studied for several decades by a variety of techniques, some of the most fundamental properties of FBPase are not understood at the atomic level. AMP competes with Mg^{2+} (*16*, *17*), but in crystal structures, the number of metal cations bound to the active site is insensitive to the presence of AMP at its allosteric site. Two Mn^{2+} ions or two Zn^{2+} ions bind to the active site in the presence and absence of AMP in crystal structures (*18*−*20*). The Hill coefficient for Mg^{2+} is approximately 2, but only one Mg^{2+} ion binds to the active site (*18*). Mutant structures of FBPase have been presented which have dramatically altered kinetic properties, yet their corresponding crystallographic structures deviate in only trivial ways from that of the wild-type enzyme (*21*, *22*). Recently, mutations of residues in loop 52−72 have resulted in dramatic changes in the functional properties of FBPase (*23*), yet the corresponding loop in all crystal structures is disordered (*15*, *18*−*22*, *24*−*28*).

Reported below is a crystallographic study of wild-type FBPase in a complex of F6P, P_i, and Zn^{2+}. The crystallographic structure is the first instance of a complete, product complex of FBPase. Loop 52−72, disordered in all prior crystallographic structures of FBPase, has moved into the active site and makes numerous hydrophobic contacts and hydrogen bonds with other residues important to the functional properties of the enzyme. Among the new interactions is a salt link between Asp68 and Arg276, which is stabilized by Zn^{2+}, bound to the putative K^+ activation site. The structure provides new insights regarding not only K^+ activation but also the essential role played by Arg276 in the structural organization of the active site. The structure also serves as a basis for new mechanisms of catalysis and allosteric regulation of FBPase.

[†] This work was supported in part by National Institutes of Health Research Grant NS 10546 and National Science Foundation Grants MCB-9603595 and MCB-8316244. This is Journal Paper J-17923 of the Iowa Agriculture and Home Economics Experiment Station, Ames, Project 3191.

[‡] Coordinates and structure factors for the structure described in this paper have been deposited with the Brookhaven Protein Data Bank (accession number 1BFL).

* Corresponding author. Telephone: (515) 294-6116. Fax: (515) 294-0453. E-mail: honzatko@iastate.edu.

[§] Present address: Howard Hughes Medical Institute, Baylor College of Medicine, Houston, TX 77030.

[1] Abbreviations: FBPase, fructose-1,6-bisphosphatase; P_i, phosphate; F6P, fructose 6-phosphate; $F16P_2$, fructose 1,6-bisphosphate; $F26P_2$, fructose 2,6-bisphosphate; 2,5-AnG-1,6-P_2, 2,5-anhydroglucitol 1,6-bisphosphate; SDS−PAGE, sodium dodecyl sulfate−polyacrylamide gel electrophoresis.

S0006-2960(98)01112-X CCC: $15.00
Published on Web 07/29/1998

Table 1: Statistics of Data Collection and Refinement

resolution limit (Å)	2.27
no. of reflections	145 331
no. of unique reflections	31 028
completeness (%) of data set	90.0
completeness (%) of last shell (2.27−2.4 Å)	56.4
R_{sym}[a]	5.5
no. of reflections used in refinement[b]	22 526
no. of atoms[c]	6974
no. of solvent sites	266
R-factor[d]	0.186
R_{free}[e]	0.282
mean *B* for protein (Å^2)	14.3
root-mean-squared deviations	
bond lengths (Å)	0.011
bond angles (Å)	1.68
dihedral angles (deg)	24.5
improper dihedral angles (Å)	1.35

[a] $R_{sym} = \Sigma_j\Sigma_i I_{ij} - \langle I_j\rangle/\Sigma_j\Sigma_i I_{ij}$, where *i* runs over multiple observations of the same intensity and *j* runs over all crystallographicly unique intensities. [b] All reflections from 5 to 2.27 Å and where $F_{obs} > 0$ not used in the calculation of R_{free}. [c] Includes hydrogen atoms linked to polar atoms. [d] *R*-factor $= \Sigma F_{obs} - F_{calc}/\Sigma F_{obs}$, where $F_{obs} > 0$. [e] *R*-factor based upon 10% of the data randomly chosen and not used in refinement.

EXPERIMENTAL PROCEDURES

Expression and Purification of Wild-Type FBPase. FBPase-deficient *Escherichia coli* strain DF657 [*tonA22, ompF627(T$_2$R), relA1, pit10, spoT1,* Δ*(fbp)287*; Genetic Stock Center at Yale University, New Haven, CT] was employed in the expression of recombinant wild-type porcine FBPase. Expression and purification of FBPase followed the procedures of Burton et al. (*29*) with minor modification. After centrifugation to remove cell debris, the supernatant fluid was subjected to heat treatment, 30−70% ammonium sulfate precipitation, Sephadex G-100 column chromatography, and CM-Sepharose column chromatography. FBPase eluted as a single peak with CM-Sepharose chromatography, using a NaCl gradient (20 to 400 mM) in 10 mM malonate at pH 6.

Crystallization of the Product Complex. Crystals of FBPase were grown by the method of hanging drops. Equal parts of a protein solution [FBPase (10 mg/mL), KP_i at pH 7.4 (10 mM), Tris-malonate at pH 7.4 (2.5 mM), $ZnCl_2$ (5 mM), and F6P (5 mM)] and a precipitant solution [Tris-malonate at pH 7.4 (2.5 mM) and polyethylene glycol 3350 (6% w/v)] were combined to give a 4 μL droplet. Wells contained 500 μL of the precipitant solution. Crystals with the dimensions 0.4 mm × 0.4 mm × 0.3 mm, belonging to the space group $P2_12_12$ (a = 52.34 Å, b = 166.77Å, and c = 82.82 Å), grew in approximately 3 days at 4 and 37 °C. Structures of crystals grown at 37 and 4 °C are identical. Data presented below are from a crystal grown at 37 °C.

Data Collection. Data were collected at Iowa State University on a rotating anode/Siemens area detector at 100 K, using CuKα radiation passed through a graphite monochoromator. Data were reduced by XENGEN (*30*) and were 90% complete to a resolution of 2.3 Å (Table 1).

Structure Determination. Crystals grown for this study are not isomorphous with respect to any known crystal form reported in previous studies of FBPase. Hence, a structure determination was initiated by molecular replacement. Using programs of the CCP4 (*31*) package and the canonical R state for FBPase (accession identifier 1FBE), rotation and translation functions (*32*, *33*) provided dominant peaks and an unambiguous solution (initial *R*-factor of 0.50). Rigid-body refinement followed by one cycle of simulated annealing [using XPLOR (*34*)] reduced the the *R*-factor to 0.31.

Model Building and Refinement. The electron density map resulting from the above molecular replacement solution revealed an extensive region of strong electron density, which did not correspond to any part of previous FBPase models. Residues 52−72 were built into this electron density along with conformational adjustments to residues 22−27, 122−127, and 267−272, using the program XTALVIEW (*35*) and a Silicon Graphics workstation (Indigo2 XL). Added to each independent subunit were three Zn^{2+} atoms, two molecules of P_i (active site and AMP site), and one molecule of F6P. (Ligands and metal cations were removed from the model used in molecular replacement and the first cycle of simulated annealing. Hence, loop 52−72, the zinc cations, P_i, and F6P were fit to an omit map.) Two models were generated for the $3Zn^{2+}$−product complex which differed from each other in the choice of F6P anomer. The resulting models underwent one round of refinement using XPLOR (*34*) with force constants and parameters of stereochemistry from Engh and Huber (*36*). A cycle of refinement consisted of slow cooling from 2000 to 300 K in steps of 25 K, followed next by 120 cycles of conjugate gradient minimization, and finally by the refinement of individual *B*-parameters with restraints of 1.5 Å^2 on nearest neighbor and next to nearest neighbor main chain atoms, 2.0 Å^2 on nearest neighbor side chain atoms, and 2.5 Å^2 on next to nearest neighbor side chain atoms.

In subsequent cycles of refinement, water molecules were fit to a difference electron density of 2.5σ or better and were added until no significant decrease was evident in R_{free}. Included in the final model were water molecules which make suitable donor−acceptor distances to each other and the protein and have *B*-parameters of less than 47 Å^2.

RESULTS

General Features of the $3Zn^{2+}$−Product Complex of FBPase. Wild-type FBPase used in crystallization experiments suffered no proteolytic degradation and, on the basis of SDS−PAGE (data not shown), is greater than 95% pure. Coordinates and structure factors have been deposited with the Brookhaven Protein Data Bank (accession code 1BFL). Statistics for data collection and refinement are given in Table 1. Uncertainty in coordinates is approximately 0.25 Å. The stereochemistry of the model is generally better than what is typical for a structure with a nominal resolution of 2.3 Å, as determined by PROCHECK (*37*). Thermal parameters vary from 7.0 to 49 Å^2. The model begins with interpretable electron density at Thr12 and continues without interruption to Ala335. Weak electron density is present for residues before Thr12, but the interpretation of that density is ambiguous. The electron density associated with residues 22−27 (loop connecting helices H1 and H2) is weak, as reflected by high thermal parameters. The rest of the polypeptide chain, however, is covered by substantial electron density.

The crystal form presented here has not been reported in prior investigations of FBPase. The space group ($P2_12_12$)

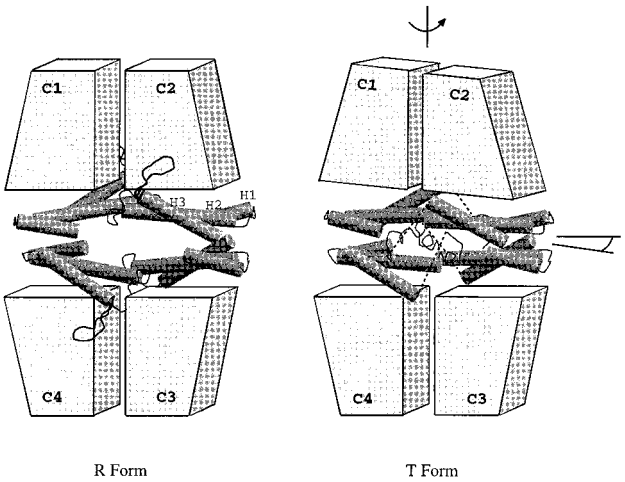

FIGURE 1: Schematic of R and T state tetramers of FBPase as defined by the $3Zn^{2+}$−product complex in the context of previous FBPase structures. Gray prisms represent residues 90−335 of subunits C1−C4. Shown explicitly are helixes H1−H3 as shaded cylinders. A 17° rotation of the dimer C1−C2 relative to the dimer C3−C4 is the major quaternary conformational change. In the R state conformer, loop 52−72, connecting helix H2 to helix H3, is ordered, whereas the same loop becomes disordered in the T state (dashed line). This figure was drawn in part with RASTER3D (*47*).

is identical to that associated with the canonical T state confomation (*25*), but the unit cell parameters differ (a = 52.34 Å, b = 166.77 Å, and c = 82.82 Å as opposed to $a \cong$ 61.0 Å, $b \cong$ 166.5 Å, and $c \cong$ 80.0 Å for canonical T state structures). As with previous FBPase crystals in space group $P2_12_12$, the asymmetric unit consists of the C1 and C2 subunits of the tetramer (Figure 1); a crystallographic 2-fold axis coincides with the molecular 2-fold axis that relates the C1 and C4 subunits. Cα's related by noncrystallographic symmetry show a root-mean-square deviation of approximately 0.2 Å, regardless of whether the AMP and/or the FBP domain is used as a basis of superposition. (Residues 1−199 and 200−335 comprise the AMP and FBP domains, respectively.) Noncrystallographic restraints were not used in refinement so that the root-mean-square deviation above is another measure of coordinate uncertainty. No pair of Cα's related by noncrystallographic symmetry deviate by more than 1.4 Å after superposition, and only for the disordered loop 22−27 do the discrepancies exceed 0.7 Å. As the relative positions and orientations of the AMP and FBP domains in the subunits related by noncrystallographic symmetry are the same, either subunit can be used in structural comparisons to the canonical R and T states of FBPase.

Rigid-Body Conformational Changes. The R to T state transition entails a 17 Å rotation between dimers C1−C2 and C3−C4 (Figure 1). The enzyme here is unambiguously in the canonical R state conformation. The root-mean-square deviation in corresponding Cα's of the tetramer, excluding the loop 52−72, is 0.88 Å against the canonical R state and 2.96 Å against the canonical T state. Hence, R state conformers are now available in two different crystal forms. Superposition of the $3Zn^{2+}$−product complex onto the canonical R state, using Cα atoms of either the FBP or AMP domain as the basis for superposition, yields similar values for root-mean-square deviations (Table 2). The AMP and FBP domains exhibit root-mean-square deviations approximately 0.15 Å lower if the same domain is used as the basis

Table 2: Root-Mean-Square Deviations (in Angstroms) between Cα's of Selected Structural Elements of the $3Zn^{2+}$−Product Complex and the Canonical R and T States of FBPase after Superpostion Based on Selected Cα's of the FBP Domain or AMP Domain

structural element	FBP domain[a]	AMP domain[b]
R state[f] *vs* product complex		
FBP domain[a]	0.50	0.63
AMP domain[b]	0.63	0.48
helix H1[c]	1.68	1.40
helix H2[d]	0.53	0.35
helix H3[e]	0.65	0.42
T state[g] *vs* product complex		
FBP domain[a]	0.33	0.66
AMP domain[b]	0.55	0.47
helix H1[c]	1.81	1.51
helix H2[d]	1.06	1.05
helix H3[e]	0.62	0.41

[a] Residues 201−335, excluding residues 267−272. [b] Residues 90−200, excluding residues 122−127. [c] Residues 12−22. [d] Residues 28−50. [e] Residues 74−89. [f] Protein Data Bank entry 1FBE. [g] Protein Data Bank entry 1FPI.

of superposition and comparison (Table 2). The discrepancy may be a consequence of a small difference in the relative orientation of the AMP and FBP domains in the canonical R state and the product complex. Whether this difference in orientation has functional significance, however, is doubtful. Indeed, the small discrepancy above may stem from differences in packing environments of the two crystal forms.

The AMP domain rotates by approximately 2° relative to the FBP domain in the R to T state transition (*27*). The 2° rotation putatively transforms the functional active site (which lies at the interface between AMP and FBP domains) to the inhibited active site (*20*). Superposition of the $3Zn^{2+}$−product complex onto the canonical T state of FBPase, using (as above) the AMP or FBP domains as a basis of superposition, reveals again a small discrepancy in root-mean-square deviations (Table 2). As in the case of the canonical R state, the relative position and orientation of the AMP and FBP domains in the product complex do not differ appreciably from those of the canonical T state (Figure 2). Again, it is unclear whether small differences in the relative orientation and position of the AMP and FBP domains in various crystal forms of FBPase are functionally significant or just a consequence of different packing environments. Non-rigid-body conformational changes described below may play a more significant role in determining the functional state of FBPase.

Non-Rigid-Body Conformational Changes. Superpositions of the $3Zn^{2+}$−product complex onto the canonical R and T state reveal significant differences for Cα atoms 12−72, 122−127, and 267−272 (Table 2 and Figure 2). Helix H1 (residues 12−22) adopts a different position relative to the corresponding elements in the canonical R and T state. The connecting element between helix H1 and H2 (residues 23−27) is disordered in the $3Zn^{2+}$−product complex (as in the canonical R state), so conformational differences here may be simply a consequence of coordinate uncertainty. The corresponding element is ordered, however, in the canonical T state, reflecting the stabilizing influence of bound AMP. The relative position of helix H2 (residues 28−51) in the $3Zn^{2+}$−product complex corresponds to that of the canonical R state, being displaced relative to helix H2 of the T state

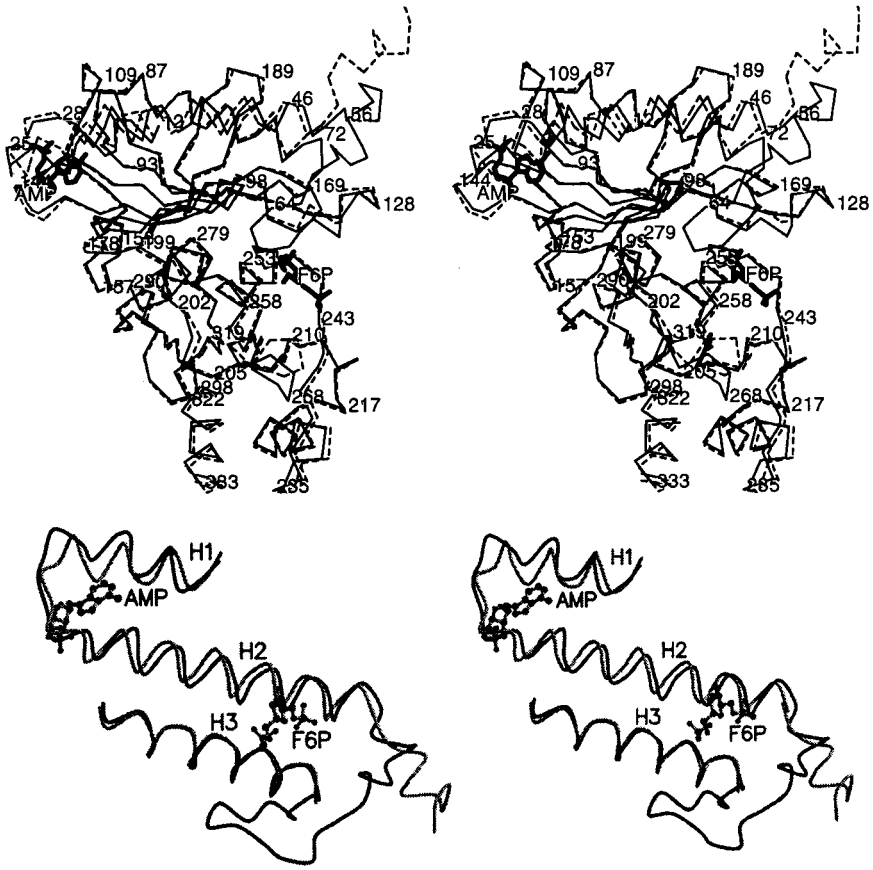

FIGURE 2: Superposition of the $3Zn^{2+}$−product complex (solid line) onto the canonical T state of FBPase (dashed line). Cα's of residues belonging to the central β-sheet of the AMP domain (residues 90−199, excluding residues 122−127) are the basis for the superposition. Differences due to the rigid-body motion of the AMP domain relative to the FBP domain are small. However, residues 12−72 (helix H1, helix H2, and loop 52−72), 122−127 (helix H4), and 267−272 undergo significant conformational change (top). Helix H2 of the $3Zn^{2+}$−product complex (solid line) moves 0.9 Å along its axis relative to the T state (gray line), and loop 52−72 goes from a state of disorder to an ordered conformation (bottom). The top orientation of the subunit corresponds to that of subunit C4 in Figure 1. The bottom is related to the top illustration by a 90° rotation about the horizontal axis. This figure was drawn with MOLSCRIPT (*48*).

by approximately 0.9 Å along the helix axis (Figure 2). Residues 52−72 of the $3Zn^{2+}$−product complex are ordered (Figure 2), whereas the corresponding element in the canonical R and T states is disordered. Residues 52−61 of the canonical T state take up a decidedly different conformation relative to the same residues of the $3Zn^{2+}$−product complex (Figure 2). Helix H4 of the $3Zn^{2+}$−product complex adopts an ordered conformation which differs from that of the poorly ordered H4 in the canonical R and T state structures. Finally, the conformation of loop 267−272 of the $3Zn^{2+}$−product complex differs from that of the canonical R and T states.

Helix H1, loop 52−72, helix H4, and loop 267−272 have conformations which are not observed in either the canonical R or T state. In fact, the ordering of loop 52−72 and conformational displacements in helix H1, helix H4, and loop 262−267 may be coupled phenomena. We suggest that the canonical R state of FBPase represents an incomplete transition, showing principally the displacement in helix H2, but not the displacements involving helix H1, loop 52−72, helix H4, and loop 262−267.

Interactions of Loop 52−72. In its ordered conformation, loop 52−72 interacts predominantly with the AMP domain of its own subunit (Table 3 and Figure 3). It makes significant contacts as well with the FBP domain of its own subunit and the AMP domain of the subunit related by noncrystallographic symmetry (that is, a C1−C2 or C3−C4 contact in Figure 1). Leu56 and Tyr57 pack onto a

Table 3: Selected Donor−Acceptor Distances Involving Atoms of Loop 52−72[a]

atom from loop 52−72	contact atom	distance (Å)
Ala54 N	Lys50 O	2.97
His55 N	Ala51 O	2.99
	Gly52 O	3.05
Leu56 N	Ala51 O	2.78
Tyr57 O	Lys72 NZ	2.67
Gly58 O	Lys72 N	3.02
Ala60 N	Val70 O	2.70
Ser62 N	Gln69 OE1	3.00
Ser62 O	Gln69 OE1	2.78
	Val70 N	2.63
Asn64 N	Asp68 O	3.01
Asn64 O	Gly67 N	2.73
Asn64 OD1	Thr66 OG1	3.10
	Gly67 N	3.11
	Asp68 N	2.80
Asn64 ND1	Glu98 OE1	3.40
Thr66 O	Arg313 NH2	2.99
Thr66 OG1	Arg276 NH1	2.83
Asp68 OD2	Arg276 NH1	3.20
	Zn^{2+} (site 3)	2.19
Lys71 N	Asp74 OD1	2.67
Lys71 O	Asp74 N	2.86
Lys71 NZ	Ser123 OG	2.91

[a] Distances taken from polypeptide chain B.

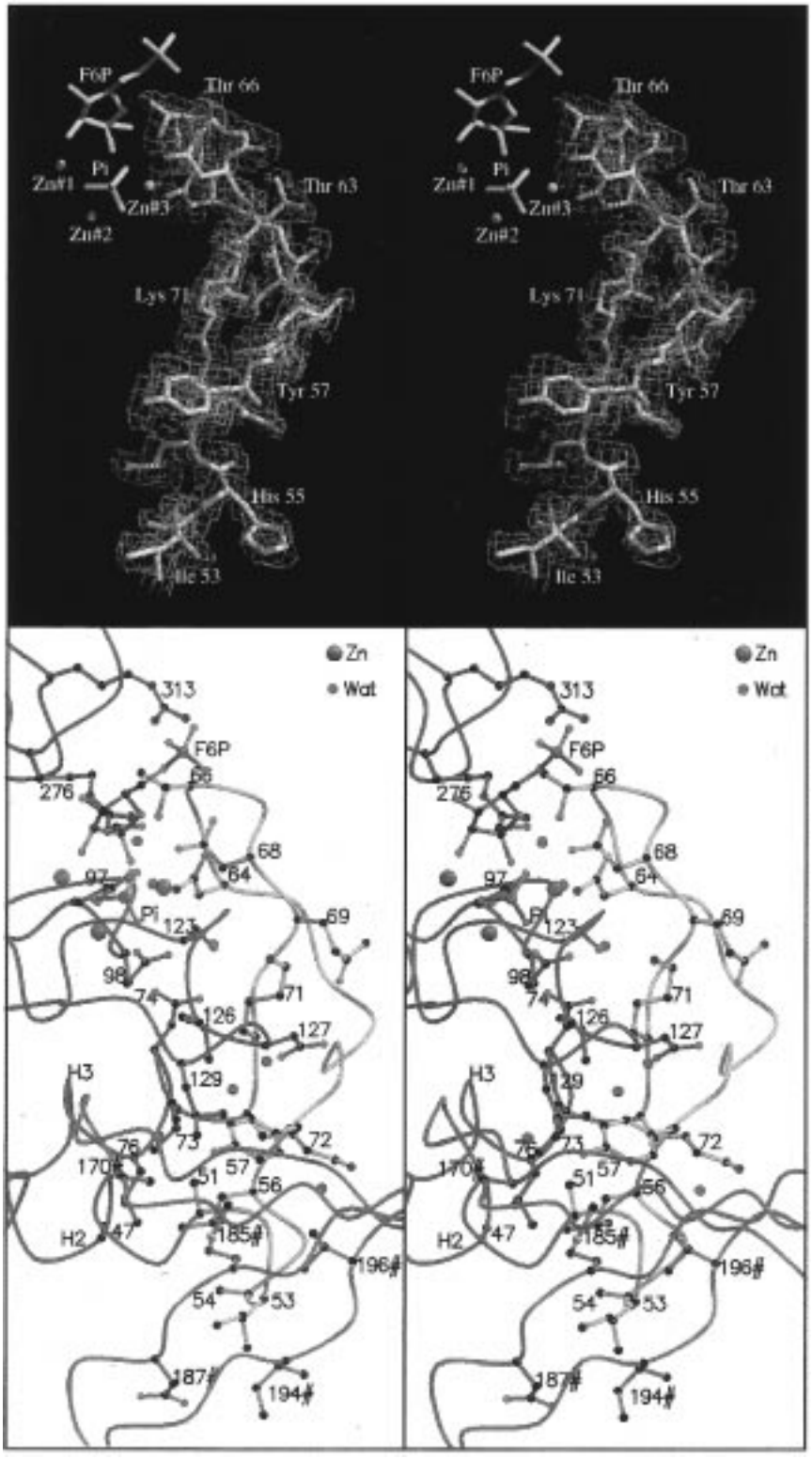

FIGURE 3: Loop 52−72 in its engaged conformation. Well-defined electron density in an omit map covers loop 52−72 at a 3σ contour level and a cutoff radius of 1 Å (top). Loop 52−72 (yellow) interacts with the AMP and FBP domains of the same subunit (blue) and the AMP domain of a symmetry-related subunit (purple) (bottom). This figure was drawn with XTALVIEW (*35*), MOLSCRIPT (*48*), and RASTER3D (*47*).

hydrophobic patch at the surface of two separate AMP domains, and in so doing form new hydrophobic clusters (Figure 3). The side chain of Leu56 is within 4.5 Å of the side chains of Ala47, Ala51, Ala54, Leu73, and Leu76, complementing the hydrophobic interactions between helix H2 and H3. The side chain of Tyr57 is within 4.5 Å of those of Ala51, Ile126, Leu129, Ala170#, and Met185#; its interactions with Ile126 and Leu129 may be responsible in part for the conformational ordering of helix H4 (the symbol # designates the subunit related by noncrystallographic symmetry).

In addition to the aforementioned hydrophobic contacts, numerous polar contacts presumably stabilize the observed conformation of loop 52−72. Backbone amides 54, 55, and

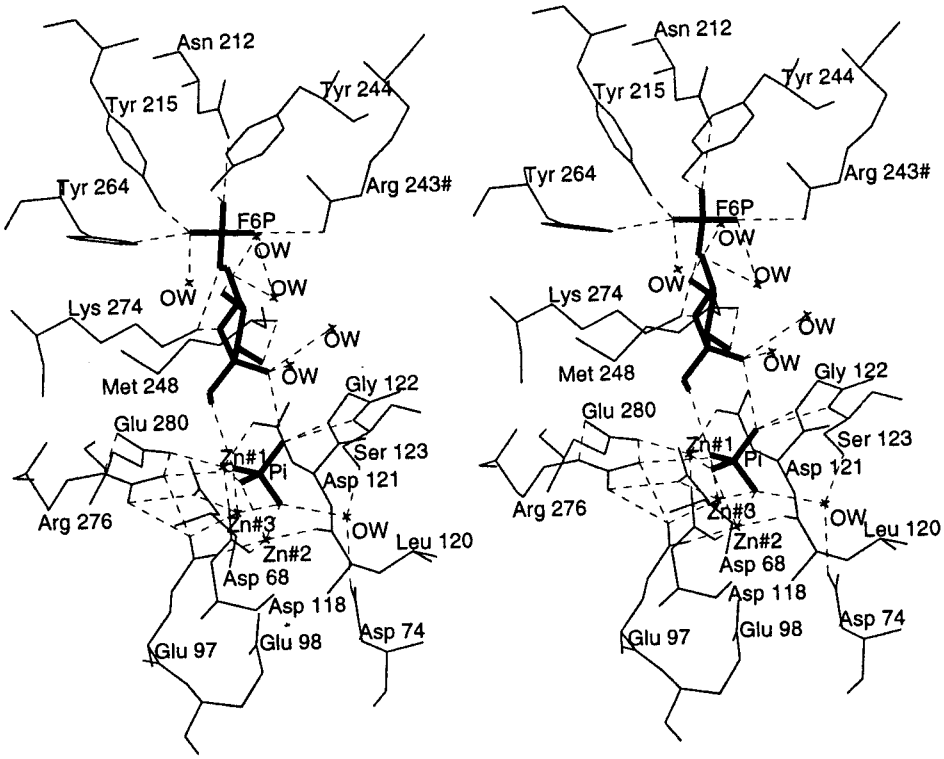

FIGURE 4: Stereoview of the active site. Donor−acceptor interactions are indicated by dashed lines. This figure was drawn with XTALVIEW (*35*).

56 hydrogen bond with backbone carbonyls 50, 51, and 52 (Table 3). The model for the canonical R state ends at Ile53. Hence, the above backbone interactions are absent in the disordered conformation of the loop. Asn64 hydrogen bonds weakly with Glu98, which is an essential residue for catalysis at neutral pH (*38*). Asp68 coordinates to zinc at site 3, but perhaps of greater significance is its hydrogen bond with Arg276, a residue important in catalysis (*39*). The side chains of Lys71 and Ser123 hydrogen bond with each other, and in addition, backbone carbonyls 58 and 71 interact with backbone amides 72 and 74, respectively. Perhaps more significant, however, is the hydrogen bond between backbone amide 71 and the side chain of Asp74. Mutations of Asp74 reduce k_{cat} by 50000-fold (*23*). Interactions involving residues 71, 74, and 123 are absent in the disordered conformation of loop 52−72.

We have up to now described loop 52−72 as existing in two conformational states (ordered and disordered), but in fact, 10 donor−acceptor interactions among residues 57−70 (Table 3) could stabilize the observed conformation for this portion of the loop even in its disordered state. Hence, a relatively rigid element of secondary structure defined here by residues 57−70 could be hinged to the AMP domain by flexible elements spanning residues 50−56, 71, and 72. Given the above as a possible scenario, we prefer the terminology engaged and disengaged (instead of ordered and disordered, respectively) in referring to the conformational state of loop 52−72.

Ligand and Divalent Cation Interactions. The zinc cations occupy metal binding sites 1−3 defined in previous studies of FBPase (*18*, *28*), but the coordination of each metal ion differs. The side chain of Asp121 is in the inner sphere of the Zn^{2+} at site 1 for the product complex (Table 4 and Figure 4), as opposed to other R state structures where it is 2.8 Å from the metal atom (*18*). The coordination at site 2 involves two oxygen atoms from P_i instead of a single oxygen from the 1-phosphoryl group of 2,5-AnG-1,6-P_2 (*18*). Zn^{2+} at site 3 coordinates two oxygen atoms of P_i, and one oxygen each from Asp68 and Glu280. In the $3K^+$−2,5-AnG-1,6-P_2−AMP complex (*28*), the K^+ at site 3 did not interact with Asp68 as loop 52−72 is disordered, but does interact with Glu97 and the 1-phosphoryl group of the inhibitor.

F6P and P_i in this structure retain many of the interactions (Table 4 and Figure 4) observed for F16P_2 and 2,5-AnG-1,6-P_2 in previous structures (*18*), but with some significant differences. The β-anomer of F6P provides the best fit to the electron density of the $3Zn^{2+}$−product complex. The α-anomer of F6P can account for most of the electron density; however, its 1-OH group must be positioned out of electron density and away from the P_i molecule to avoid steric conflict, and even then, C1 of the α-anomer of F6P makes a close contact (less than 2.5 Å) with O1 of P_i. The corresponding contact for the β-anomer is a strong hydrogen bond between the 2-OH of F6P and P_i (Table 4). The P_i molecule participates in coordinate bonds to all three zinc cations and hydrogen bonds to the 1- and 2-OH groups of the F6P molecule (Table 4 and Figure 4). The P_i molecule hydrogen bonds as well to backbone amides 122 and 123 and to the Arg276. The $3Zn^{2+}$−product complex fundamentally differs from the 2,5-AnG-1,6-P_2 complexes (*18*) in the tight packing of its active site. Indeed, the three cations, the products, and interacting side chains exhibit a complex network of hydrogen bonds (Figure 4), which restricts the conformational freedom of the products. The absence of conformational freedom in the active site of the $3Zn^{2+}$−product complex rivals that of the hydrophobic cores of the AMP and FBP domains, as measured by averaged thermal parameters.

Table 4: Selected Distances between Ligands and the Active Site[a]

ligand atom	contact atom	distance (Å)
Zn^{2+} (site 1)	Asp118 OD1	2.04
	Asp121 OD1	2.20
	Glu280 OE1	2.17
	P_i O1	1.88
Zn^{2+} (site 2)	Glu97 OE1	2.13
	Asp118 OD2	2.16
	Leu120 O	2.15
	P_i O2	2.36
	P_i O3	2.17
Zn^{2+} (site 3)	Asp68 OD2	2.19
	Glu97 OE2	2.32
	P_i O1	1.97
	P_i O3	2.57
P_i		
O1	Arg276 NH2	2.79
	Zn^{2+} (site 3)	1.97
	F6P O1	2.73
O2	Zn^{2+} (site 1)	1.88
	Zn^{2+} (site 2)	2.36
O3	Zn^{2+} (site 2)	2.17
	Zn^{2+} (site 3)	2.57
	Wat 615	2.72
O4	Gly122 N	2.86
	Ser123 N	2.89
	F6P O2	2.84
F6P		
O1	P_i O1	2.73
O2	P_i O4	2.84
	Wat 563	2.99
	Wat 592	2.71
O3	Asp121 OD1	2.71
	Met248 N	2.91
O4	Wat 538	2.74
O5	Lys274 NZ	3.05
O6	Lys274 NZ	3.03
	Wat 604	3.10
O61	Tyr215 OH	2.64
	Tyr264 OH	2.70
	Wat 576	2.87
O62	Arg243[b] NH2	2.82
	Wat 604	2.57
O63	Asn212 ND2	2.95
	Tyr244 OH	2.72

[a] Distances taken from polypeptide chain B. [b] Residue belongs to polypeptide chain A.

DISCUSSION

Model for Allosteric Regulation. The $3Zn^{2+}$−product complex, in conjunction with structures of the canonical T state, is the basis here for a new model of catalytic regulation for FBPase. The principal feature of this new model is the participation of loop 52−72 (Figure 5). Essentially all but one of the regulatory properties of FBPase can be explained in the context of a two-state subunit. AMP cooperativity is the only property necessarily linked to the tetramer.

The new R state subunit of FBPase at neutral pH has loop 52−72 engaged with the AMP and FBP domains as described above. When metal sites 1 and 2 are occupied and when $F16P_2$ is bound, loop 52−72 closes onto the active site. Interactions between loop 52−72 and the rest of the tetramer putatively position Asp74 so that it can abstract a proton from a water molecule bound to the cation at site 2 (*23*). Mutation of Asp74 to alanine or asparagine reduces k_{cat} by 50000-fold (*23*). In addition, the engaged conformation of loop 52−72 also permits Asn64 to hydrogen bond with and orient the side chain of Glu98, which putatively works in concert with Asp74 as a catalytic base (*23*, *38*).

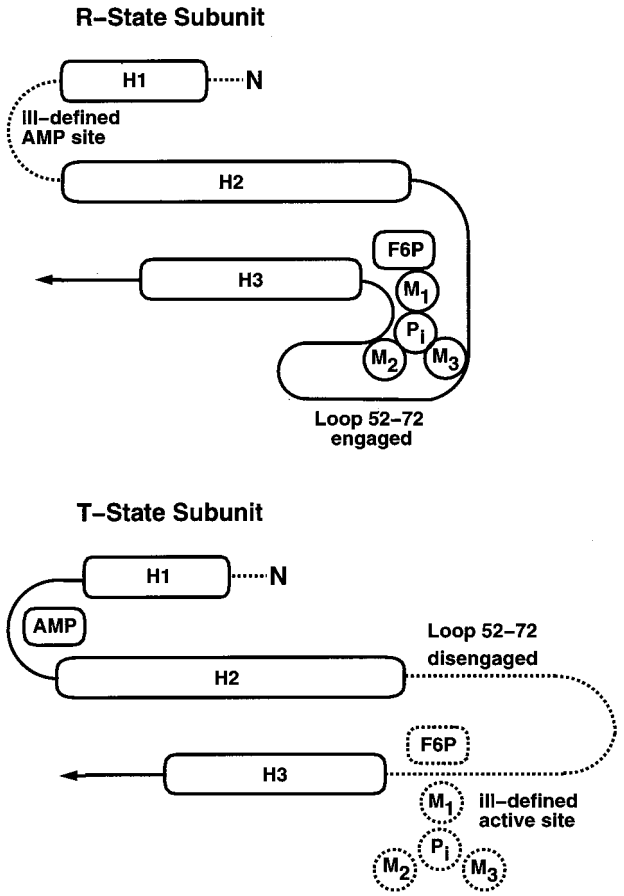

FIGURE 5: Scheme for allosteric regulation of FBPase catalysis. The engaged conformation of loop 52−72 (top) and the AMP-bound state (bottom) are antagonistic. Dashed lines represent poorly ordered structure. See the text for details.

Finally, the engaged loop also stabilizes the hydrogen bond of Asp68 with Arg276, completing the coordination site for metal 3. In the absence of a metal at site 3, Asp68 will feel the electrostatic repulsion of the 1-phosphoryl group of the substrate. That repulsive interaction can be offset by the protonation of the 1-phosphoryl group or by the presence of a cation at site 3. Hence, the structural origin of monovalent cation activation is probably the stabilization of the Asp68···Arg276 hydrogen bond by neutralization of electrostatic charge on the 1-phosphoryl group. At neutral pH, the new model accounts for the Hill coefficient of 2 for Mg^{2+}, requiring metals at sites 1 and 2.

The canonical T state subunit of FBPase is represented by the $3K^+$−2,5-AnG-1,6-P_2−AMP structure (*28*). AMP, by binding to the allosteric pocket, drives a conformational change which perturbs the position of helix H2 by a translation of 0.9 Å along its axis (Figures 2 and 5). The coupling of AMP binding and the movement of helix H2 may be indirect. For instance, AMP could bind to loop 22−27 and stabilize a conformation which favors the T state tetramer. Interactions between subunits C1 and C4 of the T state tetramer (Figure 1) then could displace helix H2. The small displacement of helix H2 putatively disengages loop 52−72 from the rest of the tetramer, which in turn perturbs Asp74 and Glu98 (catalytic base tandem). Conceivably, the disengagement of loop 52−72 in the T state will lessen the affinity of Mg^{2+} for site 1 and/or site 2. Indeed, the complex of 2,5-AnG-1,6-P_2 with Mg^{2+} (loop 52−72 disengaged) has

metal at site 1 only (*18*). Hence, the observation of competition between AMP and Mg^{2+} (*16*, *17*) may be linked to the dynamics of loop 52−72. $F26P_2$ and AMP are synergistic inhibitors of FBPase, a phenomenon which is easy to understand if AMP and $F26P_2$ both stabilize the same conformational state (disengaged loop 52−72). Indeed, the 2-phosphoryl group of $F26P_2$ does not (and evidently cannot) interact with Arg276 in crystal structures of $F26P_2$ complexes (*19*, *26*). Furthermore, the 2-phosphoryl group cannot be in the inner coordination sphere of the cation at site 3. Hence, the structural elements that contribute most to interactions with the side chain of Asp68 are not in place in $F26P_2$ complexes of FBPase.

FBPase is just one of a growing list of enzymes which employ one or more flexible loops in its biochemical function (for examples, see refs *40*−*42*). The new model for allosteric regulation of catalysis requires that loop 52−72 have at least two conformational states and that at least one of these states (the engaged conformation) be important in catalysis. Investigations of directed mutations confirm a significant role for loop 52−72 in regulation and catalysis (*23*), but why until now has loop 52−72 been disordered in all crystal structures of the R state? Perhaps, as discussed below, the R state exists in solution as a manifold of conformational states with different functional properties, and under a specific set of conditions, only one of these states is selected by the process of crystallization. On the other hand, in previous studies of the R state, crystals of FBPase were grown in the presence of F6P without metal cations (*15*, *18*), and desired ligands and cations were diffused into the resulting $P3_221$ crystal form. Crystal packing interactions of the $P3_221$ crystal form, which presumably stabilize a partially ligated conformation of FBPase, may inhibit the complete transformation to an active conformer in the presence of metal ions and substrate analogues. The crystal form presented here results from the cocrystallization of cations and a complete set of products. Crystals isomorphous with respect to those of the $3Zn^{2+}$−product complex have been grown in the presence of F6P and P_i along with Mg^{2+}, Mg^{2+} and K^+, Mg^{2+}, Zn^{2+}, and K^+, and Mn^{2+}. (Preliminary results show occupancy levels ranging from approximately 50 to 100% for the engaged conformation of loop 52−72 in the presence of Mg^{2+} alone or in combination with other metals.) No crystallization experiment in our hands involving metal cations and products, however, has resulted in the $P3_221$ crystal form of the canonical R state.

Mechanism of Catalysis. F6P and P_i are products of the forward reaction mediated by FBPase. In the presence of only Zn^{2+} at 5 mM, FBPase hydrolyzes $F16P_2$ at a rate that is approximately 70% of that in the presence of 5 mM Mg^{2+} (J.-Y. Choe and R. B. Honzatko, unpublished). The $3Zn^{2+}$−product complex then should not be far removed from a productive complex. The presence of an unambiguous product complex in the crystal structure is consistent with the reported thermodynamic equilibrium constant (K_{eq}, approximately 200 M) for the conversion of $F16P_2$ to F6P and P_i (*3*). Hence, this structure should provide some information relevant to the catalytic mechanism of FBPase.

To make the reverse reaction go, a catalytic base (catalytic acid in the forward direction) must abstract a proton from the 1-OH of F6P. If the torsion bond between C1 and C2 of F6P is rotated by 120° into an alternative staggered

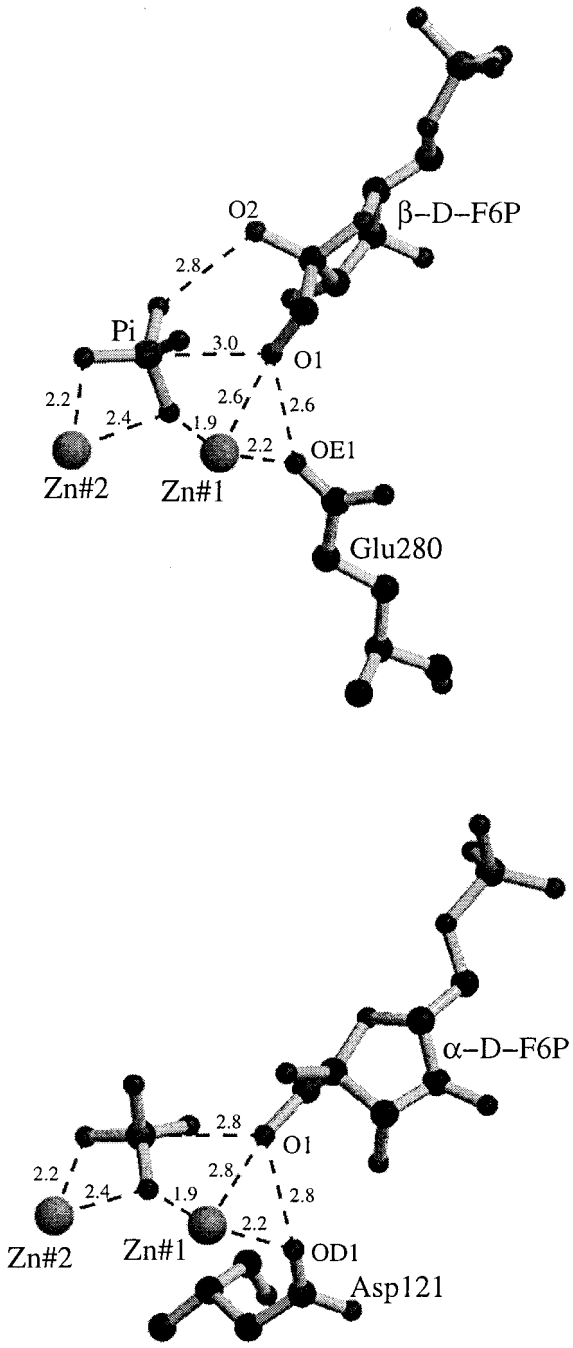

FIGURE 6: Models for early transition states of the reverse reaction of FBPase, based on the $3Zn^{2+}$−product complex. Glu280 is the putative catalytic base for the β-anomer of F6P (top), and Asp121 is the catalytic base for the α-anomer (bottom). See the text for details. This figure was drawn with MOLSCRIPT (*48*) and RASTER3D (*47*).

conformation, a favorable geometry exists between the zinc cation at site 1, the side chain of Glu280, the P_i molecule, and the 1-OH of F6P (Figure 6). As the hydrogen atom of the 1-OH group bonds with Glu280, the O1 atom can form a transient coordinate bond with Zn^{2+} at site 1. Such interactions should activate the 1-OH group as a nucleophile in the reverse reaction. Furthermore, the 1-OH group takes up near-perfect, in-line geometry with respect to the phosphorus atom of P_i and the leaving group (oxygen atom of P_i coordinated to the Zn^{2+} at site 2). The leaving oxygen could be protonated directly by Asp74 and Glu98 (catalytic acid tandem in the reverse reaction), but more likely, the water

molecule hydrogen bonded with Asp74 (Figure 4) would mediate proton transfer. The structure-based mechanism described above would require that Asp74, Glu98, Glu280, and metal cations at sites 1 and 2 be essential for catalysis, which is consistent with investigations in kinetics and directed mutation. Also, the 2-OH group of F6P hydrogen bonds with P_i , an interaction which may promote the close approach of the O1 atom of F6P and the phosphorus atom of P_i. Analogues of $F16P_2$ which lack a 2-OH group are not substrates for FBPase (*43*).

The above model, however, may be at odds with other studies regarding the conformationally active form of the substrate. Putatively, the α-anomer of $F16P_2$ is necessary for catalysis (*44*), even though the *β*-anomer is favored thermodynamically in solution (*45*) and may bind more tightly to the active site (*43*). Although the α-anomer of F6P cannot account for electron density at the active site (see above), a model for the α-anomer can be positioned into the cavity of the active site of the $3Zn^{2+}$−product complex. The active site can then be relaxed to the model for the α-anomer by energy minimization to ensure a set of allowable interactions (Figure 6). The O1 atom of the α-anomer of F6P is 2.8 Å from the zinc cation at site 1 and 2.8 Å from the side chain of Asp121. The O1 atom of the α-anomer is in line with the phosphate atom and the oxygen atom of P_i coordinated to the cation at site 2. Asp121 would serve as the catalytic base in the reverse reaction, consistent with its putative role as a catalytic acid in the forward reaction (*18*).

Clearly, this issue of anomeric specificity is not resolved, as any crystallographic structure can provide only an approximation of the transition state. The structure reported here and/or previously published structures may be dead-end complexes of FBPase. The kinetic evidence supporting the α-anomer as the substrate (*44*, *46*), however, is equally indirect and relates to catalysis by FBPase in the presence of Mn^{2+}. Indeed, in the presence of Mg^{2+}, data from rapid quenching kinetics infer utilization of both α- and *β*-anomers of $F16P_2$ (*3*). Furthermore, no data (aside from this study) regarding the anomeric specificity of the reverse reaction catalyzed by FBPase are available. Differences in reaction rates catalyzed by FBPase in the presence of Zn^{2+}, Mn^{2+}, and/or Mg^{2+} may stem from fundamentally different catalytic mechanisms. Under in vivo conditions, different metal combinations at the active site may result in a mixture of FBPases capable of using both anomers of the substrate. If so, the structure of the $3Zn^{2+}$−product complex may reflect the mechanism of one of many active forms of FBPase, distinguished principally by the cations located at the active site. At the very least, the $3Zn^{2+}$−product complex should motivate further investigation of the regulatory and catalytic mechanisms of FBPase in the presence of various cation and ligand combinations.

REFERENCES

1. Krebs, H. A. (1963) in *Advances in Enzyme Regulation* (Weber, G., Ed.) Vol. 1, pp 385−400, Pergamon Press Ltd., London.
2. Marcus, F. (1981) in *The Regulation of Carbohydrate Formation and Utilization in Mammals* (Veneziabe, C. M., Ed.) pp 269−290, University Park Press, Baltimore.
3. Benkovic, S. J., and de Maine, M. M. (1982) *Adv. Enzymol. Relat. Areas Mol. Biol. 53*, 45−82.
4. Hers, H. G., and Hue, L. (1983) *Annu. Rev. Biochem. 52*, 617−653.
5. Tejwani, G. A. (1983*) Adv. Enzymol. Relat. Areas Mol. Biol. 54*, 121−194.
6. Pilkus, S. J., El-Maghrabi, M. R., and Claus, T. H. (1988) *Annu. Rev. Biochem. 57*, 755−783.
7. Taketa, K., and Pogell, B. M. (1965*) J. Biol. Chem. 240*, 651−662.
8. Nimmo, H. G., and Tipton, K. F. (1975*) Eur. J. Biochem. 58*, 567−574.
9. Stone, S. R., and Fromm, H. J. (1980) *Biochemistry 19*, 620−625.
10. McGrane, M. M., El-Maghrabi, M. R., and Pilkus, S. J. (1983) *J. Biol. Chem. 258*, 10445−10454.
11. Liu, F., and Fromm, H. J. (1988) *J. Biol. Chem. 263*, 9122−9128.
12. Sola, M. M., Oliver, F. J., Salto, R., Gutierrez, M., and Vargas, A. M. (1993) *Int. J. Biochem. 25*, 1963−1968.
13. Zhang, R., Villeret, V., Lipscomb, W. N., and Fromm, H. J. (1996) *Biochemistry 35*, 3038−3043.
14. Nimmo, H. G., and Tipton, K. F. (1975) *Eur. J. Biochem. 58*, 575−585.
15. Ke, H., Zhang, Y., Liang, J.-Y., and Lipscomb, W. N. (1991) *Proc. Natl. Acad. Sci. U.S.A. 88*, 2989−2993.
16. Scheffler, J. E., and Fromm, H. J. (1986) *Biochemistry 25*, 6659−6665.
17. Liu, F., and Fromm, H. J. (1990) *J. Biol. Chem. 265*, 7401−7406.
18. Zhang, Y., Liang, J.-Y., Huang, S., Ke, H., and Lipscomb, W. N. (1993) *Biochemistry 32*, 1844−1857.
19. Xue, Y., Huang, S., Liang, J.-Y., Zhang, Y., and Lipscomb, W. N. (1994) *Proc. Natl. Acad. Sci. U.S.A. 91*, 12482−12486.
20. Villeret, V., Huang, S., Zhang, Y., and Lipscomb, W. N. (1995) *Biochemistry 34*, 4307−4315.
21. Lu, G., Williams, M. K., Giroux, E. L., and Kantrowitz, E. R. (1995) *Biochemistry 34*, 13272−13277.
22. Lu, G., Stec, B., Giroux, E. L., and Kantrowitz, E. R. (1996) *Protein Sci. 5*, 2333−2342.
23. Kurbanov, F. T., Choe, J.-Y., Honzatko, R. B., and Fromm, H. J. (1998) *J. Biol. Chem. 273*, 17511−17516.
24. Ke, H., Thorpe, C. M., Seaton, B. A., and Lipscomb, W. N. (1989) *J. Mol. Biol. 212*, 513−539.
25. Ke, H., Liang, J.-Y., Zhang, Y., and Lipscomb, W. N. (1991) *Biochemistry 30*, 4412−4420.
26. Liang, J.-Y., Huang, S., Zhang, Y., Ke, H., and Lipscomb, W. N. (1992) *Proc. Natl. Acad. Sci. U.S.A. 89*, 2404−2408.
27. Zhang, Y., Liang, J.-Y., Huang, S., and Lipscomb, W. N. (1994) *J. Mol. Biol. 244*, 609−624.
28. Villeret, V., Huang, S., Fromm, H. J., and Lipscomb, W. N. (1995) *Proc. Natl. Acad. Sci. U.S.A. 92*, 8916−8920.
29. Burton, V. A., Chen, M., Ong, W. C., Ling, T., Fromm, H. J., and Stayton, M. M. (1993) *Biochem. Biophys. Res. Commun. 192*, 511−517.
30. Howard, A. J., Nielsen, C., and Xuong, N. H. (1985) *Methods Enzymol. 114*, 452−472.
31. Collaborative Computational Project, Number 4 (1994) *Acta Crystallogr. 15*, 24−31.
32. Crowther, R. A. (1971) in *Molecular Replacement Method* (Rossmann, M. G., Ed.) pp 173−178, Gordon and Breach, New York.
33. Crowther, R. A., and Blow, D. M. (1967) *Acta Crystallogr. 23*, 544−548.
34. Brünger, A. T. (1992) *XPLOR*, version 3.1, Yale University Press, New Haven, CT.
35. McRee, D. E. (1992*) J. Mol. Graphics 10*, 44−46.
36. Engh, R. A., and Huber, R. (1991) *Acta Crystallogr. A47*, 392−400.

37. Laskowski, R. A., MacArthur, M. W., Moss, D. S., and Thornton, J. M. (1993) *J. Appl. Crystallogr. 26*, 283−291.
38. Kelly, N., Giroux, E. L., Lu, G., and Kantrowitz, E. R. (1996) *Biochem. Biophys. Res. Commun. 219*, 848−852.
39. Zhang, R., and Fromm, H. J. (1995) *Biochemistry 34*, 8190−8195.
40. Noble, M. E. M., Zeelen, J. Ph., and Wierenga, R. K. (1993) *Proteins: Struct., Funct., Genet. 16*, 311−326.
41. Fu, Z., Hu, Y., Markham, G. D., and Takusagawa, F. (1996) *J. Biomol. Struct. Dyn. 13*, 727−739.
42. Poland, B. W., Fromm, H. J., and Honzatko, R. B. (1996) *J. Mol. Biol. 264*, 1013−1027.
43. Marcus, F. (1976*) J. Biol. Chem. 251*, 2963−2966.
44. Frey, W., Fishbein, R., de Maine, M. M., and Benkovic, S. J. (1977) *Biochemistry 16*, 2479−2484.
45. Midelfort, C. F., Gupta, R. K., and Rose, I. A. (1976) *Biochemistry 15*, 2178−2185.
46. Benkovic, P. A., Bullard, W. P., de Maine, M. M., Fishbein, R., Schray, K. J., Steffens, J. J., and Benkovic, S. J. (1974*) J. Biol. Chem. 249*, 930−931.
47. Merritt, E. A., and Bacon, D. J. (1997) *Methods Enzymol. 277*, 505−524.
48. Kraulis, J. (1991) *J. Appl. Crystallgr. 24*, 946−950.

BI981112U